universe

MDPI

Article

The General Property of Tracking and Thawing Models and Their Observational Constraints

Yujie You, Qichao Qiang and Qing Gao *

School of Physical Science and Technology, Southwest University, Chongqing 400715, China
* Correspondence: gaoqing1024@swu.edu.cn

Abstract: We study the general property of the evolution of a class of scalar fields with tracking and thawing behaviors. For the tracking solutions, we show explicitly with three different potentials that, independent of initial conditions, there exists a general relation between the equation of state w_ϕ and the fractional energy density Ω_ϕ, so that the scalar field follows the same $w_\phi - \Omega_\phi$ trajectory during the evolution. The analytical approximations of the $w_\phi - \Omega_\phi$ trajectories are derived even though the analytical expression depends upon the particular form of the potential. For thawing solutions, a universal $w_\phi - \Omega_\phi$ relation exists and the relation is independent of both the particular form of the potential and the initial condition of the scalar field. Based on the derived $w_\phi - \Omega_\phi$ relation for the thawing models, we derive a tighter upper limit on $w'_\phi = dw_\phi/d\ln a$. The observational data is also used to constrain the thawing potential with the help of the universal $w_\phi - \Omega_\phi$ relation.

Keywords: quintessence field; tracking solution; thawing solution; observational constraints

1. Introduction

The observations of type Ia supernova provided the evidence to support the late time cosmic acceleration [1–3]. To explain the late time cosmic acceleration, an exotic matter component with negative pressure dubbed as dark energy is usually introduced. The observations suggested that dark energy contributes about 72% to the total energy density in the universe. The simplest candidate for dark energy is the cosmological constant, but the theoretical estimation of the value of the cosmological constant is in discrepancy with the astronomical observations by about 120 orders of magnitude [4], and the cosmological constant as dark energy candidate faces fine tuning and coincidence problems. Based on the concordance ΛCDM model, the release of Planck first year data on the measurements of the cosmic microwave background anisotropy gave the value of the Hubble constant as $H_0 = 67.3 \pm 1.2$ km/s/Mpc [5,6]. This value is in tension with the local measurement on the Hubble constant $H_0 = 73.8 \pm 2.4$ km/s/Mpc by calibrating the magnitude–redshift relation of 253 type Ia supernovae with over 600 Cepheid variables [7]. With more data and more accurate measurements, the measurement accuracy of the Hubble constant was improved greatly [7–27] and the tension became more serious [28]. For example, Planck 2018 data gave the result $H_0 = 67.4 \pm 0.5$ km/s/Mpc [25], the supernovae and H_0 for the equation of state (SH0ES) team measured the local Hubble constant as $H_0 = 73.15 \pm 0.97$ km/s/Mpc from Type Ia supernovae (SNe Ia) data by recalibrating the extragalactic distance ladder using a sample of Milky Way Cepheids with the Hubble Space Telescope photometry and Gaia EDR3 parallaxes [13]. By using the tip of the red giant branch method, the local measurements of the Hubble constant gave $H_0 = 69.8 \pm 0.6$ (stat) ± 1.6 (sys)km/s/Mpc [14]. Since the Planck results from the early Universe probe of cosmic microwave background anisotropy depend on the ΛCDM model and the local measurements from type Ia supernova standard candles suffer the zero-point calibration problem, we are still uncertain about the origin of the tension on the Hubble constant. Gravitational waves as standard sirens provide an independent method of measuring cosmological distance and the observations of

Citation: You, Y.; Qiang, Q.; Gao, Q. The General Property of Tracking and Thawing Models and Their Observational Constraints. *Universe* **2023**, *9*, 146. https://doi.org/10.3390/universe9030146

Academic Editor: Jean-Michel Alimi

Received: 19 February 2023
Revised: 27 February 2023
Accepted: 9 March 2023
Published: 11 March 2023

gravitational waves and their electromagnetic counterparts may shed light on the origin of the tension on the Hubble constant [29–31]. The first gravitational wave event GW170817 from binary neutron star merger and its counterpart GRB 170817A gave $H_0 = 70.0^{+12.0}_{-8.0}$ km/s/Mpc [32]. Combining the galaxy catalog and 47 gravitational wave events from the third LIGO-Virgo-KAGRA Gravitational-Wave Transient Catalog (GWTC-3), LIGO-Virgo-KAGRA collaborations obtained $H_0 = 68^{+8}_{-6}$ km/s/Mpc [33].

Although more astronomical observations support the late time cosmic acceleration, the question whether the cosmological constant is dark energy remains unanswered. For these reasons, dark energy is usually tackled by a dynamical scalar field called quintessence [34–37]. As discussed in [38–41], the value of the Hubble constant H_0 can be lowered by quintessence models relative to the cosmological constant. Other possibilities for dark energy such as phantom [42], quintom [43–45], tachyon [46–48], and k-essence [49] were also considered. Alternatively, the late time cosmic acceleration approach can also be explained by modifying general relativity at the cosmological scale, such as the Dvali–Gabadadze–Porrati model [50], f(R) gravity [51–54], and dRGT ghost-free massive gravity [55,56]. For a review of dark energy and alternative theories of gravity, please see Ref. [57–65].

In general, to discuss the evolution of a scalar field, we need to impose initial conditions, so it is difficult to get the property of the quintessence field from observational data. Therefore, it is worthwhile to seek the general behavior of dynamical dark energy which is independent of initial conditions. Fortunately, there exist general $w_\phi - \Omega_\phi$ trajectories for the thawing and tracking solutions [66–88]. For a wide class of quintessence potentials with the tracking solution [37,68], the equation of state parameter $w(z)$ for the quintessence varies slowly. Motivated by this behavior, Efstathiou approximated $w(z)$ as $w(z) = w_0 - \alpha \ln(1+z)$ in the redshift range $z < 4$ [89]. For a wide class of scalar fields, Chevallier–Polarski–Linder (CPL) parametrization with $w(a) = w_0 + w_a(1-a)$ [90,91] was usually used as a model-independent parametrization. Combining the generic $w_\phi - \Omega_\phi$ relations and the CPL parametrization, the degeneracy between the two parameters w_0 and w_a in the CPL parametrization can be broken by an analytical relation [87,92,93]. In this paper, we study the general property of the evolution for the tracker and thawing fields.

The paper is organized as follows. In Section 2, we discuss the reason for the same $w_\phi - \Omega_\phi$ trajectory in the tracker solution. In Section 3, we derive the $w_\phi - \Omega_\phi$ trajectories for different potentials with tracking solutions. We derived the thawing solution and obtained the constraint by using observational data for different potentials in Section 4. The conclusion is drawn in Section 5.

2. The Tracking Solution

Using the fractional energy density Ω_ϕ and the equation of state parameter $\gamma = 1 + w_\phi$, the evolution of a scalar field is determined by the following equations:

$$\Omega'_\phi = 3(\gamma_b - \gamma_\phi)\Omega_\phi(1-\Omega_\phi), \tag{1}$$

$$\gamma'_\phi = (2-\gamma_\phi)(-3\gamma_\phi + |\lambda|\sqrt{3\gamma_\phi\Omega_\phi}), \tag{2}$$

$$\lambda' = -\sqrt{3\gamma_\phi\Omega_\phi}\lambda|\lambda|(\Gamma - 1), \tag{3}$$

where "$\prime$" represents the derivative with respect to $\ln a$, $w_b = [(1/3)a_{eq}/a]/[1 + a_{eq}/a]$ is the equation of state for the background, $\lambda = -V^{-1}dV/d\phi$ is the roll parameter, and $\Gamma = \lambda^{-2}V^{-1}d^2V/d\phi^2$ is the tracker parameter. With these dynamical Equations (1)–(3), we first discuss the behavior of tracking solution. To get the tracking solution, the potential $V(\phi)$ must satisfy the condition $\Gamma \geq 1$ [68] so that the absolute value of the roll parameter

$|\lambda|$ either decreases with time or remains a constant. When the tracking solution is reached, $\gamma_\phi' = 0$, the tracker condition [68]:

$$\gamma_\phi = 1 + w_\phi = \frac{1}{3}\lambda^2 \Omega_\phi \tag{4}$$

is satisfied, the flow parameter $F = \gamma_\phi/(\Omega_\phi \lambda^2) = 1/3$ and $\beta = -1 + (1 - w_\phi)/\sqrt{12F} = -\gamma_\phi/2$. If $\gamma_\phi'' \approx 0$, then γ_ϕ is nearly a constant [68,74]:

$$w_\phi = \frac{w_b(1 - \Omega_\phi) - 2(\Gamma - 1)}{2\Gamma - 1 - \Omega_\phi}. \tag{5}$$

It is clear that w_ϕ is not a constant in general. To get a nearly constant w_ϕ, we must require that Ω_ϕ is negligibly small and the tracker parameter $\Gamma - 1$ is nearly a constant for the tracking solution. The exponential potential has $\Gamma = 1$, and the inverse power-law potential $V(\phi) = V_0 \phi^{-\alpha}$ has $\Gamma = 1 + 1/\alpha$, so they have the tracking behavior. If $\Omega_\phi \approx 0$, then:

$$w_\phi \approx w_\phi^{trk} = \frac{w_b - 2(\Gamma - 1)}{2\Gamma - 1}, \tag{6}$$

and the roll parameter λ must be large so that the tracker condition can be satisfied. If $\Gamma - 1$ is not a constant, then it must be either large or small, so that $w_\phi \approx -1$ or $w_\phi \approx w_b$. For example, the potential $V(\phi) = V_0 \exp[-(3\phi)^{2/3}/2]$ has large $\Gamma - 1 = \lambda^2$ and the potential $V(\phi) = V_0 \exp(1/\phi)$ has small $\Gamma - 1 = 2/\sqrt{\lambda}$. In summary, the tracking solution satisfies the two conditions (4) and (6) initially, and the necessary conditions for the tracker behavior to occur are: when the tracker condition (4) is satisfied, the fractional energy density Ω_ϕ should be negligible which requires that the initial value of $|\lambda|$ should be big enough and the roll parameter $|\lambda|$ either decreases with time or remains a constant.

Now let us discuss the dependence of the tracking solution on initial conditions. We consider two different initial conditions: (i) If the initial value of the fractional energy density $\Omega_{\phi i}$ is not too small or the initial value of the roll parameter λ_i is large enough so that $\lambda_i^2 > 3\gamma_{\phi i}/\Omega_{\phi i}$, then from Equation (2), we see that whatever the initial value of w_ϕ, γ_ϕ will always increase toward 2 until $\gamma_\phi' = 0$. If $\gamma_\phi > \gamma_b$, then Equation (1) tells us that Ω_ϕ will start to decrease because $\Omega_\phi' < 0$. Once Ω_ϕ decreases to a small value so that $\lambda^2 < 3\gamma_\phi/\Omega_\phi$, Equation (2) tells us that $\gamma_\phi' < 0$, then γ_ϕ decreases toward to zero and Ω_ϕ starts to increase if $\gamma_\phi < \gamma_b$. Although λ decreases, it can be larger than $3\gamma_\phi/\Omega_\phi$ if $\gamma_\phi \to 0$ because Ω_ϕ increases, so γ_ϕ will increase again. When the equation of state parameter γ_ϕ increases away from zero, it will satisfy the relation $\lambda^2 < 3\gamma_\phi/\Omega_\phi$ and w_ϕ will reach the tracker behavior (6), perhaps with several oscillations. However, if the roll parameter decreases too quickly, which can be seen in the potential $V(\phi) = V_0 \exp[-(3\phi)^{2/3}/2]$ with $\Gamma = 1 + \lambda^2$ and $\lambda' \propto \lambda^4$, then there is no tracker solution with a nearly constant w_ϕ because λ is too small when the tracker condition is satisfied. The reason is as follows: If λ_i is small, then $\Omega_{\phi i}$ cannot be too small and Ω_ϕ may reach 1 very quickly, so there is no tracker solution with nearly constant w_ϕ. (ii) If the initial value $\Omega_{\phi i}$ or λ_i is small, and the condition $\lambda_i^2 < 3\gamma_{\phi i}/\Omega_{\phi i}$ is satisfied initially, then independent of the initial value $\gamma_{\phi i}$, Equations (1) and (2) tell us that the equation of state parameter γ_ϕ decreases toward 0 and the fractional energy density Ω_ϕ starts to increase if $\gamma_\phi < \gamma_b$, then the analysis is similar to that in the first case (i). If λ_i is small, then Ω_ϕ always increases although $\Omega_{\phi i}$ is small, and it will reach 1 soon, so there is no tracker solution with nearly constant w_ϕ during the matter domination. However, the current values of Ω_ϕ, λ, and w_ϕ are determined by their initial values. These analyses tell us that there is no tracker solution with nearly constant w_ϕ if the initial value of λ is small because Ω_ϕ reaches 1 very quickly and the scalar field becomes dominant. When Ω_ϕ reaches 1, then the evolution of Ω_ϕ stops and the dynamical Equations (1)–(3) reduce to the equations for γ_ϕ and λ. From Equations (2) and (3), we get a relation between w_ϕ and λ. Since $\Omega_\phi \approx 1$ and w_ϕ approaches -1 asymptotically,

if Γ is a function of λ, then the relation between w_ϕ and λ becomes universal which is independent of the initial conditions, so the relation between w_ϕ and w'_ϕ is also universal when $w_\phi \to -1$. For example, there exists the attractor solution $\Omega_\phi = 1$, $w_\phi = -1$ and $\lambda = 0$ for the potential $V(\phi) = V_0 \exp[-(3\phi)^{2/3}/2]$.

Since the tracking conditions (4) and (6) are the initial conditions for the tracking solution, if the same initial value of Ω_ϕ is given, then w_ϕ, Ω_ϕ, and λ will follow the same trajectory, and independent of the initial conditions we will have the same $w_\phi - \Omega_\phi$ trajectory for the tracking solution. Although $w_\phi - \Omega_\phi$ trajectory is the same, the exact values of w_ϕ and Ω_ϕ at a moment are still determined by the initial conditions.

3. The Analysis of Different Potentials

For the inverse power-law potential $V(\phi) = V_0\phi^{-\alpha}$, the tracker parameter $\Gamma = 1 + \alpha^{-1}$, and the critical point $(\Omega_{\phi c}, \gamma_{\phi c}, \lambda_c) = (1, 0, 0)$ is a stable point. As $\Omega_\phi \to 1$, both γ_ϕ and λ decrease to zero asymptotically, $\gamma_\phi \approx \lambda^2/3 + 2\lambda^4/(9\alpha)$, $\sqrt{\lambda^2\Omega_\phi} \approx \sqrt{3\gamma_\phi}(1 - \gamma_\phi/\alpha)$ and $\gamma'_\phi \approx -3(2 - \gamma_\phi)\gamma_\phi^2/\alpha$. When the scalar field starts to catch up the background, the $w_\phi - \Omega_\phi$ trajectory can be approximated with a linear relation [75,94]:

$$\Omega_\phi = \frac{1 - 2w_i + 4w_i^2}{(1 - w_i^2)w_i}(w_\phi - w_i), \tag{7}$$

where $w_i = w_\phi^{trk}$. Therefore:

$$\sqrt{\lambda^2\Omega_\phi} - \sqrt{3\gamma_\phi} \approx -\frac{\gamma_b - \gamma_i}{\gamma_i}\frac{\gamma_\phi\sqrt{3\gamma_\phi}}{2 - \gamma_\phi}\left(1 - \frac{\gamma_\phi}{\gamma_i}\right). \tag{8}$$

Substitute the above relation (8) into Equations (1) and (2), we derive the approximate relation:

$$\Omega_\phi = \left[1 - \frac{(1 - w_i^2)w_i}{1 - 2w_i + 4w_i^2}\frac{1}{\gamma_i - \gamma_\phi}\left(\frac{\gamma_\phi}{\gamma_i}\right)^{1/2 + \gamma_i\gamma_b/4(\gamma_b - \gamma_i)} \exp\left[\frac{\gamma_i\gamma_b}{\gamma_i - \gamma_b}\left(\frac{1}{\gamma_\phi} - \frac{1}{\gamma_i}\right)\right]\right]^{-1}. \tag{9}$$

The $\Omega_\phi - w_\phi$ trajectories for the inverse power-law potential along with the analytical approximation (9) are shown in Figure 1. It is clear that the analytical result (9) approximates the $\Omega_\phi - w_\phi$ trajectory well, especially for smaller α as shown in Figure 1, and the inverse power-law potential $V(\phi) = V_0\phi^{-2}$ is excluded by observational data.

For the potential $V(\phi) = V_0 \exp(1/\phi)$, $\Gamma = 1 + 2/\sqrt{\lambda}$. The tracking solution starts with $\gamma_\phi^{trk} = \gamma_b/(1 + 4/\sqrt{\lambda}) \approx \gamma_b$ because λ is large due to the tracker condition. As $\gamma_\phi \to 0$ and $\Omega_\phi \to 1$, we have $\lambda\sqrt{\Omega_\phi} \approx \sqrt{3\gamma_\phi}[1 - 2(3\gamma_\phi)^{3/4}/3]$ and $\gamma'_\phi \approx -4(3\gamma_\phi)^{7/4}/3$. The $w_\phi - \Omega_\phi$ relation for the tracking solution can be approximated with:

$$\Omega_\phi = \left[1 + 3\gamma_\phi^{1/4}(1 - \gamma_\phi)^{-15/2}\exp[-(3\gamma_\phi)^{1/4} - (3\gamma_\phi)^{-3/4}]\right]^{-1}. \tag{10}$$

The $\Omega_\phi - w_\phi$ trajectory and the analytical approximation (10) are shown in Figure 1. As seen from Figure 1, the analytical relation (10) approximates the trajectory well and the potential $V(\phi) = V_0 \exp(1/\phi)$ is consistent with observational data.

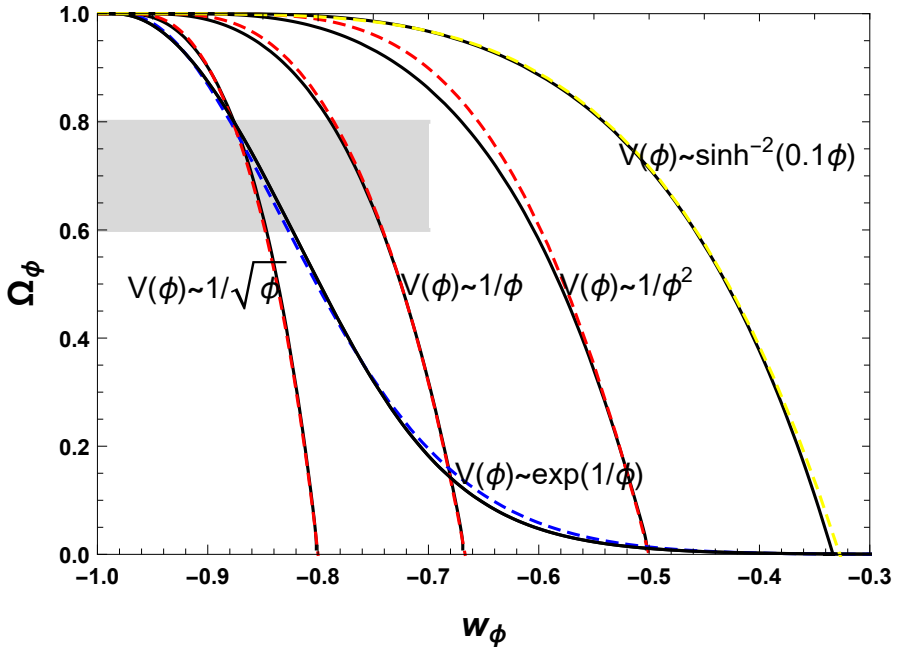

Figure 1. The $w_\phi - \Omega_\phi$ trajectories for the inverse power-law potential $V(\phi) \sim \phi^{-\alpha}$, the potential $V(\phi) \sim \exp(1/\phi)$, and the potential $V(\phi) = V_0 \sinh^{-2}(0.1\phi)$ with the tracking behavior. The dashed lines denote the analytical approximations (9)–(11). The shaded region is the allowed region by astronomical observations, $\Omega_{\phi 0} \in (0.6, 0.8)$ and $w_{\phi 0} < -0.7$.

For the potential $V(\phi) = V_0 \sinh^{-\beta}(\alpha\phi)$, the tracker parameter $\Gamma = 1 + 1/\beta - \alpha^2\beta/\lambda^2$. By setting $\Omega'_\phi = \gamma'_\phi = \lambda' = 0$, we obtain the following critical points. Point C1 with $(\Omega_{\phi C1}, \gamma_{\phi C1}, \lambda_{C1}) = (1, 2, \alpha\beta)$: it exists for all parameters, the point is a saddle point when $\lambda > \sqrt{6}$ and unstable when $\lambda < \sqrt{6}$. Point C2 with $(\Omega_{\phi C2}, \gamma_{\phi C2}, \lambda_{C2}) = (0, 2, \lambda)$: it exists for all parameters and the point is an unstable point. Point C3 with $(\Omega_{\phi C3}, \gamma_{\phi C3}, \lambda_{C3}) = (0, 0, \lambda)$: it exists for all parameters and the point is a saddle point for $-1 < w < 1$. Point C4 with $(\Omega_{\phi C4}, \gamma_{\phi C4}, \lambda_{C4}) = (1, 0, \lambda)$: it exists for all parameters and the point is a stable point only when $\lambda = 0$. Point C5 with $(\Omega_{\phi C5}, \gamma_{\phi C5}, \lambda_{C5}) = (3\gamma_b/\lambda^2, \gamma_b, \alpha\beta)$: the existence condition is $\lambda^2 > 3(1 + w_\phi)$, the point is a stable point for $3(1 + w_\phi) < \lambda^2 < 24(1 + w_\phi)^2/(7 + 9w_\phi)$ and saddle point when $\lambda^2 > 24(1 + w_\phi)^2/(7 + 9w_\phi)$. Point C6 with $(\Omega_{\phi C6}, \gamma_{\phi C6}, \lambda_{C6}) = (1, \alpha^2\beta^2/3, \alpha\beta)$: the existence condition is $\lambda^2 < 6$, the point is a stable point for $\lambda^2 < 3(1 + w_\phi)$ and saddle point when $3(1 + w_\phi) < \lambda^2 < 6$. If we choose $\alpha = 0.1$ and $\beta = 2$, the $w_\phi - \Omega_\phi$ relation for the tracking solution can be approximated with:

$$\Omega_\phi = 1 - 28 \times 3^{-3/2} \gamma_\phi^{17/4}. \tag{11}$$

The $\Omega_\phi - w_\phi$ trajectory and the analytical approximation (11) are shown in Figure 1. As seen from Figure 1, the analytical relation (11) approximates the trajectory well and the model $V(\phi) = V_0 \sinh^{-2}(0.1\phi)$ is excluded by observational data.

Although we derived analytical approximations for the $\Omega_\phi - w_\phi$ trajectories, it seems to be different for different potentials, and the tracking behavior depends on the particular form of the potential, so it is difficult to reconstruct the general property of the tracker potential from observational data. However, the situation is different for the thawing solution.

4. The Thawing Solution

For the thawing solution, w_ϕ starts with the initial value -1 and starts to increase. From Equation (3), it is easy to see that λ will keep to be a constant when $w_\phi = -1$. Taking the approximation $\gamma_\phi \ll 1$ and $\lambda \approx \lambda_i$, we get [88]:

$$\begin{aligned} \frac{d\gamma_\phi}{d\Omega_\phi} &= \frac{-6\gamma_\phi + 2\lambda\sqrt{3\gamma_\phi\Omega_\phi}}{3\gamma_b\Omega_\phi(1-\Omega_\phi)}, \\ \gamma_\phi &= \frac{\lambda_i^2}{3}\left(1+\frac{1}{2}\gamma_b\right)^{-2}\Omega_\phi(1-\Omega_\phi)^{2/\gamma_b} \\ &\quad {}_2F_1^2\left(\frac{1}{\gamma_b}+\frac{1}{2}, \frac{1}{\gamma_b}+1, \frac{1}{\gamma_b}+\frac{3}{2}; \Omega_\phi\right), \end{aligned} \tag{12}$$

where ${}_2F_1(a,b,c,x)$ is the hypergeometric function. Note that this approximation is invalid when $\gamma_\phi \sim 1$. If we take $\gamma_b = 1$, then we recover the familiar $w_\phi - \Omega_\phi$ relation [81,92]:

$$\begin{aligned} \gamma_\phi =& \frac{\lambda_i^2}{3}\left[\frac{1}{\sqrt{\Omega_\phi}} - \left(\frac{1}{\Omega_\phi}-1\right)(\tanh^{-1}\sqrt{\Omega_\phi})\right]^2 \\ =& (1+w_0)\left[\frac{1}{\sqrt{\Omega_\phi}} - \left(\frac{1}{\Omega_\phi}-1\right)\tanh^{-1}(\sqrt{\Omega_\phi})\right]^2 \\ & \times \left[\frac{1}{\sqrt{\Omega_{\phi 0}}} - (\Omega_{\phi 0}^{-1}-1)\tanh^{-1}\sqrt{\Omega_{\phi 0}}\right]^{-2}. \end{aligned} \tag{13}$$

Note that the last equality also holds for thawing phantom models [78,92]. For thawing phantom models with the potentials $V(\phi) \sim \phi^6$, $V(\phi) \sim \phi^2$, $V(\phi) \sim \phi^{-2}$, and $V(\phi) \sim \exp(-\lambda\phi)$, it was explicitly shown that the analytical result (13) gives the behavior of $w(a)$ [78]. Therefore, we can use $w(a)$ given by Equation (13) to approximate thawing scalar fields including quintessence and phantom. If γ_ϕ is near zero, the scalar field is not much different from the cosmological constant, then we can approximate the dynamics of the thawing field by the SSLCPL model [87,92] with $w(a) = w_0 + w_a(1-a)$ and:

$$w_a = 6(1+w_0)\frac{(\Omega_{\phi 0}^{-1}-1)[\sqrt{\Omega_{\phi 0}} - \tanh^{-1}(\sqrt{\Omega_{\phi 0}})]}{\Omega_{\phi 0}^{-1/2} - (\Omega_{\phi 0}^{-1}-1)\tanh^{-1}(\sqrt{\Omega_{\phi 0}})}. \tag{14}$$

Although we discuss quintessence field only, the SSLCPL model can also approximate the thawing phantom fields.

As $\Omega_\phi \to 0$ and $w_\phi \to -1$, $\gamma_\phi \to \lambda_0^2\Omega_\phi/3(1+\gamma_b/2)^2$, we get the flow parameter $F = 1/3(1+\gamma_b/2)^2$ and $\beta = \gamma_b/2$, the results are the same as those found in [84]. If w_ϕ starts to increase during the matter domination, $\gamma_b = 1$ and $F = 4/27$. Therefore, $4/27 \le F \le 1/3$ for the thawing solution, a tighter upper limit $w'_\phi \le 3(1-w_\phi^2)/2$ is then obtained. As discussed in [88], the approximation (13) works better for smaller λ_i and the $w_\phi - \Omega_\phi$ relation (13) approximates the trajectory for the power-law potential better than that for the pseudo-Nambu Goldstone boson potential.

With the approximation (14), we use the 740 spectroscopically confirmed type Ia supernovae data from three years of the SDSS-II supernovae survey and SNLS3 supernovae data [95], the combination of *Planck* 2013 results on the measurements of the cosmic microwave background power spectra with the nine-year WMAP polarization low-multipole likelihood data [5,6,96], the 8 baryon acoustic oscillation data from the 6 dFGS survey, the baryon oscillation spectroscopic survey, the SDSS survey and the WiggleZ dark energy survey [97–101], and the 21 Hubble parameter $H(z)$ data [102–105] to constrain $w_{\phi 0}$ and $\Omega_{\phi 0}$, and the results are shown in Figure 2. As discussed above, the approximation (14) holds for both quintessence and phantom thawing fields, so the 2σ constraint

$-1.23 < w_{\phi 0} < -0.85$ applies for both quintessence and phantom thawing fields. From Figure 2, we also see that the 2σ bound on the roll parameter is $|\lambda_i| = 1.013$ for the quintessence thawing field and $|\lambda_i| = 1.199$ for the phantom thawing field. From the marginalized 95% contours of $w_{\phi 0}$ and $\Omega_{\phi 0}$ obtained in Figure 2, we reconstruct the thawing potential $V(\phi)$ by using the following relations:

$$\left(\frac{d\phi}{d\ln a}\right)^2 = 3m_{pl}^2\Omega_\phi(a)|1+w(a)|, \tag{15}$$

$$V(a) = \frac{1}{2}\rho_{cr0}(1-w(a))\Omega_\phi(a)(H(a)/H_0)^2, \tag{16}$$

where $m_{pl} = (8\pi G)^{-1/2}$ and the current critical density $\rho_{cr0} = 3m_{pl}^2H_0^2$. The reconstructed potential is shown in Figure 3. From Figure 3, we see that the power-law potential $V(\phi) = V_0\phi^{0.8}$ is consistent with the observational data. The power-law potential $V(\phi) = V_0\phi^{0.8}$ as a inflationary model is also consistent with the measurements on the cosmic microwave background anisotropy. We also find that the potential $V(\phi) = V_0\phi^{0.7}$ is consistent with the 2σ upper bound and the potential $V(\phi) = V_0\phi^{1.1}$ is consistent with the 2σ lower bound.

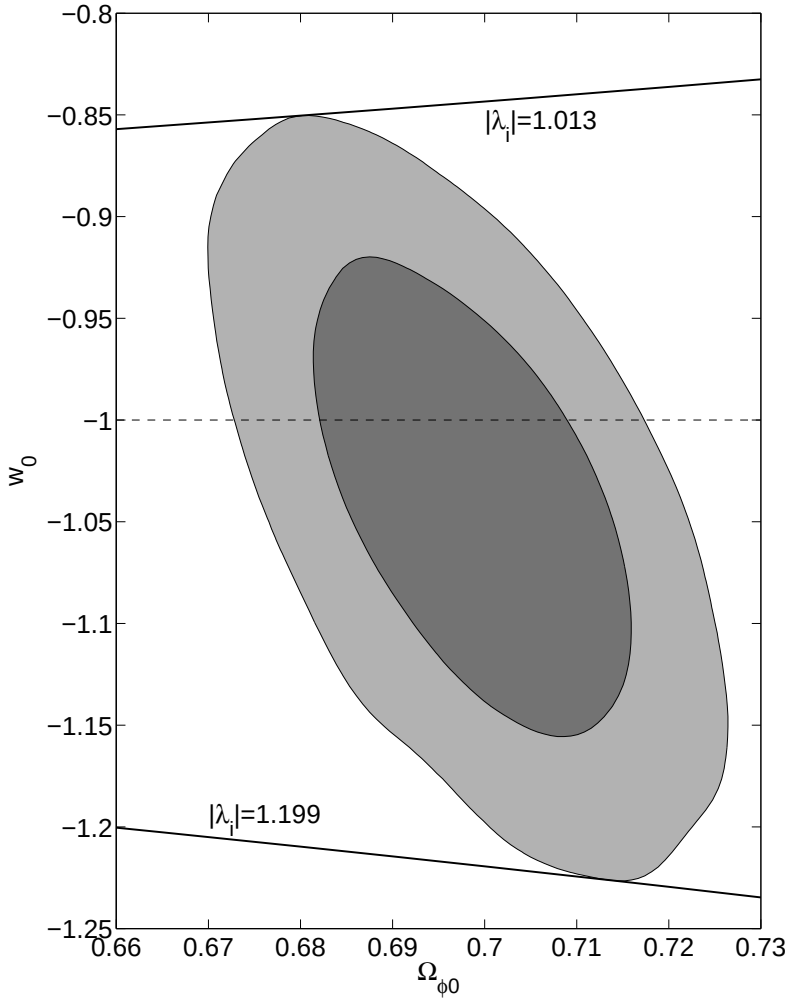

Figure 2. The marginalized 68% and 95% confidence contours of $w_{\phi 0}$ and $\Omega_{\phi 0}$ from observational data. The solid lines denote the analytical relation (13).

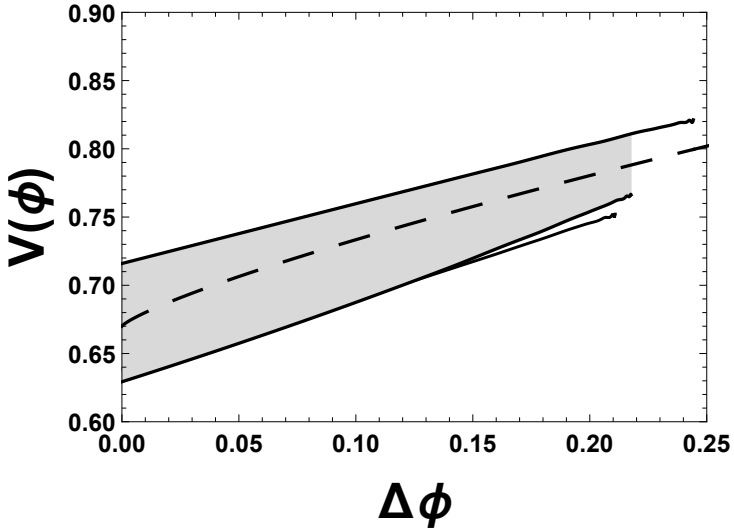

Figure 3. The 2σ constraint on quintessence thawing potentials. The potential is in the unit of the current critical density ρ_{cr0} and $\Delta\phi$ is the difference between the scalar field ϕ and its current value ϕ_0. The dashed lines denotes the power-law potential $V(\phi) \sim \phi^{0.8}$.

5. Conclusions

To guarantee an almost constant w_ϕ when the tracking solution begins, the fractional energy density Ω_ϕ should be small and the roll parameter λ must be large enough so that the tracker condition can be satisfied, and $|\lambda|$ does not increase with time. Therefore, a nearly constant tracker parameter with $\Gamma > 1$ and large initial value of the roll parameter λ are the necessary conditions for tracking solutions. Although the current value of Ω_ϕ and w_ϕ depend on the initial conditions for the tracking solutions, the $w_\phi - \Omega_\phi$ trajectory is independent of the initial conditions. We derived the analytical approximations of the $w_\phi - \Omega_\phi$ trajectory for the potentials $V(\phi) \sim \phi^{-\alpha}$ and $V(\phi) \sim \exp(1/\phi)$. Unfortunately, the analytical approximations are different for different potentials.

For the thawing solutions, $w_\phi \approx -1$ initially, the roll parameter changes very slowly and it can be approximated as a constant, a general $w_\phi - \Omega_\phi$ relation (12) is then obtained. Based on the asymptotical behavior of the $w_\phi - \Omega_\phi$ relation, we derive the tighter upper bound $w'_\phi \leq 3(1 - w_\phi^2)/2$. In general, $\Omega_{\phi 0}$ and $w_{\phi 0}$ depend on the initial conditions, so it will be difficult to constrain general scalar fields by using the observational data. However, the $w_\phi - \Omega_\phi$ trajectories for both the tracking and thawing solutions are independent of the initial conditions, so it will be easier to constrain the tracker and thawing potentials. We apply the observational data to reconstruct the thawing potential and we find that the power-law potential $V(\phi) \sim \phi^{0.8}$ is consistent with the observational data. We also find that the potential $V(\phi) = V_0\phi^{0.7}$ is consistent with the 2σ upper bound and the potential $V(\phi) = V_0\phi^{1.1}$ is consistent with the 2σ lower bound.

Author Contributions: Conceptualization, Q.G.; methodology, Q.G. and Y.Y.; formal analysis, Y.Y. and Q.Q.; writing—original draft preparation, Q.G.; writing—review and editing, Q.G.; supervision, Y.Y.; funding acquisition, Q.G. All authors have read and agreed to the published version of the manuscript.

Funding: This work is supported by the National Natural Science Foundation of China (Grant No. 12175184), the Chongqing Natural Science Foundation (CSTB2022NSCQ-MSX1324).

Data Availability Statement: Not applicable.

Conflicts of Interest: The authors declare no conflict of interest.

References

1. Perlmutter, S.; Aldering, G.; Della Valle, M.; Deustua, S.; Ellis, R.S.; Fabbro, S.; Fruchter, A.; Goldhaber, G.; Groom, D.E.; Hook, I.M.; et al. Discovery of a supernova explosion at half the age of the Universe and its cosmological implications. *Nature* **1998**, *391*, 51–54.
2. Riess, A.G.; Filippenko, A.V.; Challis, P.; Clocchiatti, A.; Diercks, A.; Garnavich, P.M.; Gillil, R.L.; Hogan, C.J.; Jha, S.; Kirshner, R.P.; et al. Observational evidence from supernovae for an accelerating universe and a cosmological constant. *Astron. J.* **1998**, *116*, 1009–1038.
3. Perlmutter, S.; Aldering, G.; Goldhaber, G.; Knop, R.A.; Nugent, P.; Castro, P.G.; Deustua, S.; Fabbro, S.; Goobar, A.; Groom, D.E.; et al. Measurements of Ω and Λ from 42 high redshift supernovae. *Astrophys. J.* **1999**, *517*, 565–586.
4. Weinberg, S. The Cosmological Constant Problem. *Rev. Mod. Phys.* **1989**, *61*, 1–23. [CrossRef]
5. Ade, P.A.R.; Aghanim, N.; Alves, M.I.R.; Armitage-Caplan, C.; Arnaud, M.; Ashdown, M.; Atrio-Barandela, F.; Aumont, J.; Aussel, H.; Baccigalupi, C.; et al. Planck 2013 results. I. Overview of products and scientific results. *Astron. Astrophys.* **2014**, *571*, A1.
6. Ade, P.A.R.; Aghanim, N.; Armitage-Caplan, C.; Arnaud, M.; Ashdown, M.; Atrio-Barandela, F.; Aumont, J.; Baccigalupi, C.; Banday, A.J.; Barreiro, R.B.; et al. Planck 2013 results. XVI. Cosmological parameters. *Astron. Astrophys.* **2014**, *571*, A16.
7. Riess, A.G.; Macri, L.; Casertano, S.; Lampeitl, H.; Ferguson, H.C.; Filippenko, A.V.; Jha, S.W.; Li, W.; Chornock, R. A 3% Solution: Determination of the Hubble Constant with the Hubble Space Telescope and Wide Field Camera 3. *Astrophys. J.* **2011**, *730*, 119; Erratum in *Astrophys. J.* **2011**, *732*, 129. [CrossRef]
8. Riess, A.G.; Macri, L.; Casertano, S.; Sosey, M.; Lampeitl, H.; Ferguson, H.C.; Filippenko, A.V.; Jha, S.W.; Li, W.; Chornock, R.; et al. A Redetermination of the Hubble Constant with the Hubble Space Telescope from a Differential Distance Ladder. *Astrophys. J.* **2009**, *699*, 539–563.
9. Efstathiou, G. H0 Revisited. *Mon. Not. R. Astron. Soc.* **2014**, *440*, 1138–1152.
10. Riess, A.G.; Macri, L.M.; Hoffmann, S.L.; Scolnic, D.; Casertano, S.; Filippenko, A.V.; Tucker, B.E.; Reid, M.J.; Jones, D.O.; Silverman, J.M.; et al. A 2.4% Determination of the Local Value of the Hubble Constant. *Astrophys. J.* **2016**, *826*, 56.
11. Riess, A.G.; Casertano, S.; Yuan, W.; Macri, L.M.; Scolnic, D. Large Magellanic Cloud Cepheid Standards Provide a 1% Foundation for the Determination of the Hubble Constant and Stronger Evidence for Physics beyond ΛCDM. *Astrophys. J.* **2019**, *876*, 85.
12. Riess, A.G.; Casertano, S.; Yuan, W.; Bowers, J.B.; Macri, L.; Zinn, J.C.; Scolnic, D. Cosmic Distances Calibrated to 1% Precision with Gaia EDR3 Parallaxes and Hubble Space Telescope Photometry of 75 Milky Way Cepheids Confirm Tension with ΛCDM. *Astrophys. J. Lett.* **2021**, *908*, L6.
13. Riess, A.G.; Breuval, L.; Yuan, W.; Casertano, S.; Macri, L.M.; Bowers, J.B.; Scolnic, D.; Cantat-Gaudin, T.; Anderson, R.I.; Reyes, M.C. Cluster Cepheids with High Precision Gaia Parallaxes, Low Zero-point Uncertainties, and Hubble Space Telescope Photometry. *Astrophys. J.* **2022**, *938*, 36.
14. Freedman, W.L. Measurements of the Hubble Constant: Tensions in Perspective. *Astrophys. J.* **2021**, *919*, 16. [CrossRef]
15. Suyu, S.H.; Bonvin, V.; Courbin, F.; Fassnacht, C.D.; Rusu, C.E.; Sluse, D.; Treu, T.; Wong, K.C.; Auger, M.W.; Ding, X.; et al. H0LiCOW—I. H0 Lenses in COSMOGRAIL's Wellspring: Program overview. *Mon. Not. R. Astron. Soc.* **2017**, *468*, 2590–2604.
16. Wong, K.C.; Suyu, S.H.; Chen, G.C.; Rusu, C.E.; Millon, M.; Sluse, D.; Bonvin, V.; Fassnacht, C.D.; Taubenberger, S.; Auger, M.W. H0LiCOW—XIII. A 2.4 per cent measurement of H0 from lensed quasars: 5.3σ tension between early- and late-Universe probes. *Mon. Not. R. Astron. Soc.* **2020**, *498*, 1420–1439.
17. Birrer, S.; Dhawan, S.; Shajib, A.J. The Hubble Constant from Strongly Lensed Supernovae with Standardizable Magnifications. *Astrophys. J.* **2022**, *924*, 2.
18. Jimenez, R.; Cimatti, A.; Verde, L.; Moresco, M.; Wandelt, B. The local and distant Universe: Stellar ages and H_0. *JCAP* **2019**, *3*, 43.
19. D'Amico, G.; Gleyzes, J.; Kokron, N.; Markovic, K.; Senatore, L.; Zhang, P.; Beutler, F.; Gil-Marín, H. The Cosmological Analysis of the SDSS/BOSS data from the Effective Field Theory of Large-Scale Structure. *JCAP* **2020**, *5*, 5.
20. Ivanov, M.M.; Simonović, M.; Zaldarriaga, M. Cosmological Parameters from the BOSS Galaxy Power Spectrum. *JCAP* **2020**, *5*, 42.
21. Colas, T.; D'amico, G.; Senatore, L.; Zhang, P.; Beutler, F. Efficient Cosmological Analysis of the SDSS/BOSS data from the Effective Field Theory of Large-Scale Structure. *JCAP* **2020**, *6*, 1.
22. Birrer, S.; Treu, T. Astrometric requirements for strong lensing time-delay cosmography. *Mon. Not. R. Astron. Soc.* **2019**, *489*, 2097–2103.
23. Camarena, D.; Marra, V. Local determination of the Hubble constant and the deceleration parameter. *Phys. Rev. Res.* **2020**, *2*, 013028.
24. Hinshaw, G.; Larson, D.; Komatsu, E.; Spergel, D.N.; Bennett, C.; Dunkley, J.; Nolta, M.R.; Halpern, M.; Hill, R.S.; Odegard, N.; et al. Nine-Year Wilkinson Microwave Anisotropy Probe (WMAP) Observations: Cosmological Parameter Results. *Astrophys. J. Suppl.* **2013**, *208*, 19.
25. Aghanim, N.; Akrami, Y.; Ashdown, M.; Aumont, J.; Baccigalupi, C.; Ballardini, M.; Banday, A.J.; Barreiro, R.B.; Bartolo, N.; Basak, S.; et al. Planck 2018 results. VI. Cosmological parameters. *Astron. Astrophys.* **2020**, *641*, A6; Erratum in *Astron. Astrophys.* **2021**, *652*, C4. [CrossRef]

26. Dainotti, M.G.; De Simone, B.; Schiavone, T.; Montani, G.; Rinaldi, E.; Lambiase, G.; Bogdan, M.; Ugale, S. On the Evolution of the Hubble Constant with the SNe Ia Pantheon Sample and Baryon Acoustic Oscillations: A Feasibility Study for GRB-Cosmology in 2030. *Galaxies* **2022**, *10*, 24.
27. Dainotti, M.G.; De Simone, B.; Schiavone, T.; Montani, G.; Rinaldi, E.; Lambiase, G. On the Hubble constant tension in the SNe Ia Pantheon sample. *Astrophys. J.* **2021**, *912*, 150.
28. Di Valentino, E.; Mena, O.; Pan, S.; Visinelli, L.; Yang, W.; Melchiorri, A.; Mota, D.F.; Riess, A.G.; Silk, J. In the realm of the Hubble tension—A review of solutions. *Class. Quant. Grav.* **2021**, *38*, 153001.
29. Schutz, B.F. Determining the Hubble Constant from Gravitational Wave Observations. *Nature* **1986**, *323*, 310–311. [CrossRef]
30. Holz, D.E.; Hughes, S.A. Using gravitational-wave standard sirens. *Astrophys. J.* **2005**, *629*, 15–22.
31. Kyutoku, K.; Seto, N. Gravitational-wave cosmography with LISA and the Hubble tension. *Phys. Rev. D* **2017**, *95*, 083525.
32. Abbott, B.P.; Abbott, R.; Abbott, T.D.; Acernese, F.; Ackley, K.; Adams, C.; Adams, T.; Addesso, P.; Adhikari, R.X.; Adya, V.B.; et al. A gravitational-wave standard siren measurement of the Hubble constant. *Nature* **2017**, *551*, 85–88.
33. Abbott, R.; Abe, H.; Acernese, F.; Ackley, K.; Adhikari, N.; Adhikari, R.X.; Adkins, V.K.; Adya, V.B.; Affeldt, C.; Agarwal, D.; et al. Constraints on the cosmic expansion history from GWTC-3. *arXiv* **2021**, arXiv:2111.03604.
34. Ratra, B.; Peebles, P.J.E. Cosmological Consequences of a Rolling Homogeneous Scalar Field. *Phys. Rev. D* **1988**, *37*, 3406. [CrossRef] [PubMed]
35. Wetterich, C. Cosmology and the Fate of Dilatation Symmetry. *Nucl. Phys. B* **1988**, *302*, 668–696.
36. Caldwell, R.R.; Dave, R.; Steinhardt, P.J. Cosmological imprint of an energy component with general equation of state. *Phys. Rev. Lett.* **1998**, *80*, 1582–1585.
37. Zlatev, I.; Wang, L.M.; Steinhardt, P.J. Quintessence, cosmic coincidence, and the cosmological constant. *Phys. Rev. Lett.* **1999**, *82*, 896–899.
38. Banerjee, A.; Cai, H.; Heisenberg, L.; Colgáin, E.O.; Sheikh-Jabbari, M.M.; Yang, T. Hubble sinks in the low-redshift swampland. *Phys. Rev. D* **2021**, *103*, L081305.
39. Lee, B.H.; Lee, W.; Colgáin, E.O.; Sheikh-Jabbari, M.M.; Thakur, S. Is local H $_0$ at odds with dark energy EFT? *JCAP* **2022**, *4*, 4.
40. Heisenberg, L.; Villarrubia-Rojo, H.; Zosso, J. Simultaneously solving the H0 and σ8 tensions with late dark energy. *Phys. Dark Univ.* **2023**, *39*, 101163.
41. Heisenberg, L.; Villarrubia-Rojo, H.; Zosso, J. Can late-time extensions solve the H0 and σ8 tensions? *Phys. Rev. D* **2022**, *106*, 043503.
42. Caldwell, R.R. A Phantom menace? *Phys. Lett. B* **2002**, *545*, 23–29.
43. Feng, B.; Wang, X.L.; Zhang, X.M. Dark energy constraints from the cosmic age and supernova. *Phys. Lett. B* **2005**, *607*, 35–41.
44. Feng, B.; Li, M.; Piao, Y.S.; Zhang, X. Oscillating quintom and the recurrent universe. *Phys. Lett. B* **2006**, *634*, 101–105.
45. Guo, Z.K.; Piao, Y.S.; Zhang, X.M.; Zhang, Y.Z. Cosmological evolution of a quintom model of dark energy. *Phys. Lett. B* **2005**, *608*, 177–182.
46. Sen, A. Tachyon matter. *JHEP* **2002**, *7*, 65.
47. Sen, A. Rolling tachyon. *JHEP* **2002**, *4*, 48.
48. Padmanabhan, T. Accelerated expansion of the universe driven by tachyonic matter. *Phys. Rev. D* **2002**, *66*, 021301.
49. Armendariz-Picon, C.; Mukhanov, V.F.; Steinhardt, P.J. A Dynamical solution to the problem of a small cosmological constant and late time cosmic acceleration. *Phys. Rev. Lett.* **2000**, *85*, 4438–4441.
50. Dvali, G.R.; Gabadadze, G.; Porrati, M. 4-D gravity on a brane in 5-D Minkowski space. *Phys. Lett. B* **2000**, *485*, 208–214.
51. Carroll, S.M.; Duvvuri, V.; Trodden, M.; Turner, M.S. Is cosmic speed - up due to new gravitational physics? *Phys. Rev. D* **2004**, *70*, 043528.
52. Nojiri, S.; Odintsov, S.D. Modified gravity with negative and positive powers of the curvature: Unification of the inflation and of the cosmic acceleration. *Phys. Rev. D* **2003**, *68*, 123512.
53. Starobinsky, A.A. Disappearing cosmological constant in f(R) gravity. *JETP Lett.* **2007**, *86*, 157–163. [CrossRef]
54. Hu, W.; Sawicki, I. Models of f(R) Cosmic Acceleration that Evade Solar-System Tests. *Phys. Rev. D* **2007**, *76*, 064004.
55. de Rham, C.; Gabadadze, G.; Tolley, A.J. Resummation of Massive Gravity. *Phys. Rev. Lett.* **2011**, *106*, 231101.
56. Gong, Y. Cosmology in massive gravity. *Commun. Theor. Phys.* **2013**, *59*, 319–323.
57. Sahni, V.; Starobinsky, A.A. The Case for a positive cosmological Lambda term. *Int. J. Mod. Phys. D* **2000**, *9*, 373–444.
58. Copeland, E.J.; Sami, M.; Tsujikawa, S. Dynamics of dark energy. *Int. J. Mod. Phys. D* **2006**, *15*, 1753–1936. [CrossRef]
59. Padmanabhan, T. Dark energy and gravity. *Gen. Rel. Grav.* **2008**, *40*, 529–564.
60. Li, M.; Li, X.D.; Wang, S.; Wang, Y. Dark Energy. *Commun. Theor. Phys.* **2011**, *56*, 525–604.
61. Nojiri, S.; Odintsov, S.D. Unified cosmic history in modified gravity: From F(R) theory to Lorentz non-invariant models. *Phys. Rept.* **2011**, *505*, 59–144.
62. Hinterbichler, K. Theoretical Aspects of Massive Gravity. *Rev. Mod. Phys.* **2012**, *84*, 671–710. [CrossRef]
63. Clifton, T.; Ferreira, P.G.; Padilla, A.; Skordis, C. Modified Gravity and Cosmology. *Phys. Rept.* **2012**, *513*, 1–189.
64. de Rham, C. Massive Gravity. *Living Rev. Rel.* **2014**, *17*, 7.
65. Nojiri, S.; Odintsov, S.D.; Oikonomou, V.K. Modified Gravity Theories on a Nutshell: Inflation, Bounce and Late-time Evolution. *Phys. Rept.* **2017**, *692*, 1–104.

66. Copeland, E.J.; Liddle, A.R.; Wands, D. Exponential potentials and cosmological scaling solutions. *Phys. Rev. D* **1998**, *57*, 4686–4690.
67. Liddle, A.R.; Scherrer, R.J. A Classification of scalar field potentials with cosmological scaling solutions. *Phys. Rev. D* **1999**, *59*, 023509.
68. Steinhardt, P.J.; Wang, L.M.; Zlatev, I. Cosmological tracking solutions. *Phys. Rev. D* **1999**, *59*, 123504. [CrossRef]
69. Brax, P.; Martin, J. The Robustness of quintessence. *Phys. Rev. D* **2000**, *61*, 103502.
70. Urena-Lopez, L.A.; Matos, T. A New cosmological tracker solution for quintessence. *Phys. Rev. D* **2000**, *62*, 081302.
71. Bludman, S.A.; Roos, M. Quintessence cosmology and the cosmic coincidence. *Phys. Rev. D* **2002**, *65*, 043503.
72. Dodelson, S.; Kaplinghat, M.; Stewart, E. Solving the Coincidence Problem: Tracking Oscillating Energy. *Phys. Rev. Lett.* **2000**, *85*, 5276–5279.
73. Johri, V.B. Search for tracker potentials in quintessence theory. *Class. Quant. Grav.* **2002**, *19*, 5959–5968. [CrossRef]
74. Rubano, C.; Scudellaro, P.; Piedipalumbo, E.; Capozziello, S.; Capone, M. Exponential potentials for tracker fields. *Phys. Rev. D* **2004**, *69*, 103510.
75. Watson, C.R.; Scherrer, R.J. The Evolution of inverse power law quintessence at low redshift. *Phys. Rev. D* **2003**, *68*, 123524.
76. Aguirregabiria, J.M.; Lazkoz, R. Tracking solutions in tachyon cosmology. *Phys. Rev. D* **2004**, *69*, 123502. [CrossRef]
77. Fang, W.; Li, Y.; Zhang, K.; Lu, H.Q. Exact Analysis of Scaling and Dominant Attractors Beyond the Exponential Potential. *Class. Quant. Grav.* **2009**, *26*, 155005.
78. Scherrer, R.J.; Sen, A.A. Thawing quintessence with a nearly flat potential. *Phys. Rev. D* **2008**, *77*, 083515. [CrossRef]
79. Scherrer, R.J.; Sen, A.A. Phantom Dark Energy Models with a Nearly Flat Potential. *Phys. Rev. D* **2008**, *78*, 067303.
80. Dutta, S.; Scherrer, R.J. Hilltop Quintessence. *Phys. Rev. D* **2008**, *78*, 123525.
81. Dutta, S.; Scherrer, R.J. Slow-roll freezing quintessence. *Phys. Lett. B* **2011**, *704*, 265–269. [CrossRef]
82. Chiba, T.; Dutta, S.; Scherrer, R.J. Slow-roll k-essence. *Phys. Rev. D* **2009**, *80*, 043517.
83. Gupta, G.; Saridakis, E.N.; Sen, A.A. Non-minimal quintessence and phantom with nearly flat potentials. *Phys. Rev. D* **2009**, *79*, 123013.
84. Chiba, T. Slow-Roll Thawing Quintessence. *Phys. Rev. D* **2009**, *79*, 083517; Erratum in *Phys. Rev. D* **2009**, *80*, 109902. [CrossRef]
85. Sen, S.; Sen, A.A.; Sami, M. The thawing dark energy dynamics: Can we detect it? *Phys. Lett. B* **2010**, *686*, 1–5.
86. del Campo, S.; Cardenas, V.H.; Herrera, R. The effect of curvature in thawing models. *Phys. Lett. B* **2011**, *694*, 279–283.
87. Gong, Y.; Gao, Q. On the effect of the degeneracy among dark energy parameters. *Eur. Phys. J. C* **2014**, *74*, 2729.
88. Gong, Y. The general property of dynamical quintessence field. *Phys. Lett. B* **2014**, *731*, 342–349. [CrossRef]
89. Efstathiou, G. Constraining the equation of state of the universe from distant type Ia supernovae and cosmic microwave background anisotropies. *Mon. Not. R. Astron. Soc.* **1999**, *310*, 842–850.
90. Chevallier, M.; Polarski, D. Accelerating universes with scaling dark matter. *Int. J. Mod. Phys. D* **2001**, *10*, 213–224.
91. Linder, E.V. Exploring the expansion history of the universe. *Phys. Rev. Lett.* **2003**, *90*, 091301. [CrossRef] [PubMed]
92. Gao, Q.; Gong, Y. Constraints on slow-roll thawing models from fundamental constants. *Int. J. Mod. Phys. D* **2013**, *22*, 1350035.
93. Gao, Q.; Gong, Y. The tension on the cosmological parameters from different observational data. *Class. Quant. Grav.* **2014**, *31*, 105007.
94. Chiba, T. The Equation of State of Tracker Fields. *Phys. Rev. D* **2010**, *81*, 023515.
95. Betoule, M.; Kessler, R.; Guy, J.; Mosher, J.; Hardin, D.; Biswas, R.; Astier, P.; El-Hage, P.; Konig, M.; Kuhlmann, S.; et al. Improved cosmological constraints from a joint analysis of the SDSS-II and SNLS supernova samples. *Astron. Astrophys.* **2014**, *568*, A22.
96. Bennett, C.L.; Larson, D.; Weil, J.L.; Jarosik, N.; Hinshaw, G.; Odegard, N.; Smith, K.M.; Hill, R.S.; Gold, B.; Halpern, M.; et al. Nine-Year Wilkinson Microwave Anisotropy Probe (WMAP) Observations: Final Maps and Results. *Astrophys. J. Suppl.* **2013**, *208*, 20.
97. Beutler, F.; Blake, C.; Colless, M.; Jones, D.H.; Staveley-Smith, L.; Campbell, L.; Parker, Q.; Saunders, W.; Watson, F. The 6dF Galaxy Survey: Baryon Acoustic Oscillations and the Local Hubble Constant. *Mon. Not. R. Astron. Soc.* **2011**, *416*, 3017–3032.
98. Percival, W.J.; Reid, B.A.; Eisenstein, D.J.; Bahcall, N.A.; Budavari, T.; Frieman, J.A.; Fukugita, M.; Gunn, J.E.; Ivezić, Ž.; Knapp, G.R.; et al. Baryon Acoustic Oscillations in the Sloan Digital Sky Survey Data Release 7 Galaxy Sample. *Mon. Not. R. Astron. Soc.* **2010**, *401*, 2148–2168.
99. Anderson, L.; Aubourg, E.; Bailey, S.; Bizyaev, D.; Blanton, M.; Bolton, A.S.; Brinkmann, J.; Brownstein, J.R.; Burden, A.; Cuesta, A.J.; et al. The clustering of galaxies in the SDSS-III Baryon Oscillation Spectroscopic Survey: Baryon Acoustic Oscillations in the Data Release 9 Spectroscopic Galaxy Sample. *Mon. Not. R. Astron. Soc.* **2013**, *427*, 3435–3467.
100. Blake, C.; Kazin, E.A.; Beutler, F.; Davis, T.M.; Parkinson, D.; Brough, S.; Colless, M.; Contreras, C.; Couch, W.; Croom, S.; et al. The WiggleZ Dark Energy Survey: Mapping the distance-redshift relation with baryon acoustic oscillations. *Mon. Not. R. Astron. Soc.* **2011**, *418*, 1707–1724.
101. Busca, N.G.; Delubac, T.; Rich, J.; Bailey, S.; Font-Ribera, A.; Kirkby, D.; Le Goff, J.M.; Pieri, M.M.; Slosar, A.; Aubourg, É.; et al. Baryon Acoustic Oscillations in the Ly-α forest of BOSS quasars. *Astron. Astrophys.* **2013**, *552*, A96.
102. Simon, J.; Verde, L.; Jimenez, R. Constraints on the redshift dependence of the dark energy potential. *Phys. Rev. D* **2005**, *71*, 123001.
103. Gaztanaga, E.; Cabre, A.; Hui, L. Clustering of Luminous Red Galaxies IV: Baryon Acoustic Peak in the Line-of-Sight Direction and a Direct Measurement of H(z). *Mon. Not. R. Astron. Soc.* **2009**, *399*, 1663–1680.

104. Stern, D.; Jimenez, R.; Verde, L.; Kamionkowski, M.; Stanford, S.A. Cosmic Chronometers: Constraining the Equation of State of Dark Energy. I: H(z) Measurements. *JCAP* **2010**, *2*, 8.
105. Moresco, M.; Cimatti, A.; Jimenez, R.; Pozzetti, L.; Zamorani, G.; Bolzonella, M.; Dunlop, J.; Lamareille, F.; Mignoli, M.; Pearce, H.; et al. Improved constraints on the expansion rate of the Universe up to z~1.1 from the spectroscopic evolution of cosmic chronometers. *JCAP* **2012**, *8*, 6.